



Evaluation of selectivity and robustness of near-infrared glucose measurements based on short-scan Fourier transform infrared interferograms

Mukire J. Wabomba^{a,1}, Gary W. Small^{a,*}, Mark A. Arnold^b

^a *Clippinger Laboratories, Department of Chemistry and Biochemistry, Center for Intelligent Chemical Instrumentation, Ohio University, Athens, OH 45701, USA*

^b *Optical Science & Technology Center and Department of Chemistry, University of Iowa, Iowa City, IA 52242, USA*

Received 30 October 2002; received in revised form 5 March 2003; accepted 10 March 2003

Abstract

The selectivity and robustness of near-infrared (near-IR) calibration models based on short-scan Fourier transform (FT) infrared interferogram data are explored. The calibration methodology used in this work employs bandpass digital filters to reduce the frequency content of the interferogram data, followed by the use of partial least-squares (PLS) regression to build calibration models with the filtered interferogram signals. Combination region near-IR interferogram data are employed corresponding to physiological levels of glucose in an aqueous matrix containing variable levels of alanine, sodium ascorbate, sodium lactate, urea, and triacetin. A randomized design procedure is used to minimize correlations between the component concentrations and between the concentration of glucose and water. Because of the severe spectral overlap of the components, this sample matrix provides an excellent test of the ability of the calibration methodology to extract the glucose signature from the interferogram data. The robustness of the analysis is also studied by applying the calibration models to data collected outside of the time span of the data used to compute the models. A calibration model based on 52 samples collected over 4 days and employing two digital filters produces a standard error of calibration (SEC) of 0.36 mM glucose. The corresponding standard errors of prediction (SEP) for data collected on the 5th (18 samples) and 7th (10 samples) day are 0.42 and 0.48 mM, respectively. The interferogram segment used for the analysis contained only 155 points. These results are compatible with those obtained in a conventional analysis of absorbance spectra and serve to validate the viability of the interferogram-based calibration.

© 2003 Elsevier Science B.V. All rights reserved.

Keywords: Near-infrared; Glucose; Interferogram; Digital filtering; Partial least-squares

1. Introduction

Significant efforts are underway to develop non-invasive blood glucose sensing technology based

on near-infrared (near-IR) spectroscopy [1–3]. The strategies currently being investigated are directed to the goal of a painless, reagentless determination that can be performed at home by diabetic patients. For this goal to be realized, two key impediments that must be overcome are (1) the design of a practical instrument for use in implementing the near-IR measurement and (2) the development of robust calibration procedures for converting the measured

* Corresponding author. Tel.: +1-750-5931748; fax: +1-750-5930148.

E-mail address: small@ohio.edu (G.W. Small).

¹ Co-author Present address: Millennium Pharmaceuticals, Inc., 256 E. Grand Avenue, South San Francisco, CA 94080, USA.

light intensities into estimated glucose concentrations.

From the standpoint of instrumental performance, a Fourier transform (FT) spectrometer offers the advantages of fast scan speed, good optical throughput, and excellent wavenumber precision. This performance is achieved through the use of an interferometer to modulate and multiplex the radiance from a broadband source. The resulting measured interferogram is de-multiplexed to a single-beam spectrum by application of the fast Fourier transform (FFT).

Unfortunately, the presence of the interferometer also introduces the characteristics of relatively high cost and fragility, both of which are problematic in an instrument designed for use at home by diabetics. These limitations arise from the presence of moving parts and the precise optical tolerances associated with the mirror drive of the interferometer.

Limiting the throw of the moving mirror offers the potential to simplify the instrumental requirements, but at the cost of decreased spectral resolution. The value of $\Delta\bar{\nu}_{1/2}$ (cm^{-1}), the full-width at half-maximum (FWHM) of the computed spectral band corresponding to an infinitely narrow line is

$$\Delta\bar{\nu}_{1/2} = \frac{0.605}{\delta_{\max}} \quad (1)$$

where δ_{\max} (cm) is the maximum displacement of the moving mirror from $\delta = 0$, the point of zero path difference (ZPD) in the interferometer [4]. This relationship assumes that the measured interferogram supplied to the FFT is sampled from $\delta = -\delta_{\max}$ to $+\delta_{\max}$.

The relationship expressed in Eq. (1) dictates that an extremely small value of δ_{\max} will produce an extremely low-resolution spectrum. The utility of decreasing the mirror throw of the interferometer is thus limited by the spectral resolution required for the glucose determination. This argument assumes, however, that the glucose concentration is estimated by use of spectra computed with the FFT and based on interferograms sampled from $\delta = -\delta_{\max}$ to $+\delta_{\max}$.

To overcome this limitation, we have proposed a two-step strategy to implement the glucose determination directly with short sections of the interferogram displaced from the ZPD point [5,6]. First, one or more bandpass digital filters are applied to reduce the frequency content of the interferogram data. Then, a glu-

cose calibration model is computed by application of partial least-squares (PLS) regression [7] to the filtered interferograms. By computing the calibration model with an interferogram segment from δ_{start} to δ_{end} with $0 < \delta_{\text{start}} < \delta_{\text{end}}$, the mirror throw can be reduced and the arguments regarding spectral resolution based on Eq. (1) are no longer relevant. In this case, the PLS algorithm is used in place of the FFT to extract frequency and intensity information from the filtered interferogram specifically for use in predicting glucose concentrations.

In previous work, this methodology was applied successfully to the determination of glucose in an aqueous buffer [5] and in an aqueous matrix containing triacetin and bovine serum albumin [6]. In the work reported here, these studies are extended by use of a six-component sample matrix in which the glucose spectral bands are severely overlapped with those of the other matrix constituents. In addition, the robustness of the interferogram-based calibration model is evaluated by use of prediction data lying outside of the time span of the calibration data.

2. Experimental

2.1. Instrumentation

The near-IR interferogram data used in this work were collected with a Nicolet Nexus 670 Fourier transform spectrometer (Thermo Nicolet Corp., Madison, WI) equipped with a tungsten-halogen source, calcium fluoride beamsplitter, and liquid nitrogen-cooled indium antimonide detector. A K-band optical interference filter (Barr Associates, Westford, MA) was placed in the optical path to isolate the 5000–4000 cm^{-1} region. Samples were contained in a demountable liquid transmission cell with a 20 mm diameter circular aperture (Model 118-3, Wilmad Glass, Buena, NJ), sapphire windows (Meller Optics, Providence, RI), and a 1.5 mm pathlength. Sample temperatures were controlled to the range of 36.9–37.1 °C by use of a refrigerated temperature bath to circulate water through an integrated jacket in the sample cell. A port in the sample cell allowed temperatures to be monitored with a type T thermocouple probe and digital thermocouple meter (Omega Engineering, Stamford, CT).

2.2. Reagents

A pH 6.86, 0.025 M phosphate buffer was prepared with distilled water using 0.025 M KH_2PO_4 and 0.025 M Na_2HPO_4 . The buffer also contained 5-fluoruracil (0.1% (w/w)) as a preservative. All samples were prepared by weighing appropriate amounts of α -D-glucose (ACS reagent, Aldrich, Milwaukee, WI), sodium L-lactate (99%, Aldrich), urea (minimum 99.5%, Sigma, St. Louis, MO), sodium L-ascorbate (>99%, Aldrich), β -alanine (>99%, Aldrich), and triacetin (approx. 99%, Sigma), and diluting with the phosphate buffer to 50 ml. Eighty mixture samples were constructed by a randomized design procedure that minimized concentration correlations among the constituents and minimized the correlation between the concentration of glucose and water. The concentration ranges for glucose, lactate, urea, ascorbate, alanine, and triacetin were 0.68–34.27, 1.18–33.34, 1.20–30.23, 1.18–22.55, 1.75–38.32, and 0.46–27.95 mM, respectively. Correlation coefficients computed between the component concentrations ranged from -0.18 to 0.11 , confirming that each species was independent.

2.3. Procedures

Interferograms were collected over 7 days in six individual sessions. For each of the six chemical constituents, Fig. 1A displays box plots that describe the concentration distributions for the samples collected on days 1–4, 5, and 7. Similar concentration distributions are indicated for these three sample groups. Fig. 1B is a bar chart that indicates the number of samples collected each day.

Double-sided interferograms containing 4096 points and based on 256 co-added scans were sampled at every two zero-crossings of the HeNe reference laser. The resulting spectral bandwidth was 7897 cm^{-1} . For each sample, three replicate interferograms were measured consecutively without removing the sample from the spectrometer. The collection of replicate interferograms for each sample was designed to allow some temperature variation to be incorporated into the data set. Even though control of the sample temperature was part of the experimental protocol, the extreme temperature sensitivity of the background water absorbance dictates that some

temperature-induced variance will still be present in the data. Triplicate interferograms of phosphate buffer were collected several times during each data collection session to allow spectra in absorbance units to be computed.

Fig. 1C displays box plots that describe the distributions of the maximum intensities in the single-beam spectra of the mixture samples collected each day. This figure reveals some drift in the single-beam intensities over the 7 days of the data collection.

For the data analysis, interferograms were transferred to Silicon Graphics Indigo² IMPACT 10000 workstations (Silicon Graphics Inc., Mountain View, CA) operating under Irix (Version 6.5, Silicon Graphics Inc.). Digital filtering and quantitative analysis calculations were performed on these systems with original software written in Fortran 77. Some calculations made use of subroutines from the IMSL library (IMSL Inc., Houston, TX). Calculations related to the factorial design used as part of the data analysis were performed with the Minitab software package (Release 13, Minitab Inc., State College, PA) implemented on a Dell Dimension 4100 personal computer (Dell Computer Corp., Austin, TX). The bandpass filter used to decimate the interferogram data was designed with the MATLAB Signal Processing Toolbox (Version 5.1, The MathWorks, Natick, MA).

2.4. Data selection

For the initial studies, the interferograms were randomly partitioned into calibration and prediction sets, containing 80% (64 samples, 192 interferograms) and 20% (16 samples, 48 interferograms), respectively, of the full data set that contained 80 samples and 240 interferograms. The calibration and prediction sets were not separated in time in order to remove the issue of instrumental drift from the evaluation of the selectivity of the interferogram-based analysis. To evaluate the effects of instrumental drift on the prediction performance of the calibration models, subsequent studies were based on the use of data from days 1 to 4 as the calibration set and days 5 and 7 as the prediction set. This split of the data corresponded to the use of the first 65% of the samples collected for calibration and the last 35% for prediction. This subsetting strategy allowed sufficient samples for use in building the calibration model, while providing a separa-

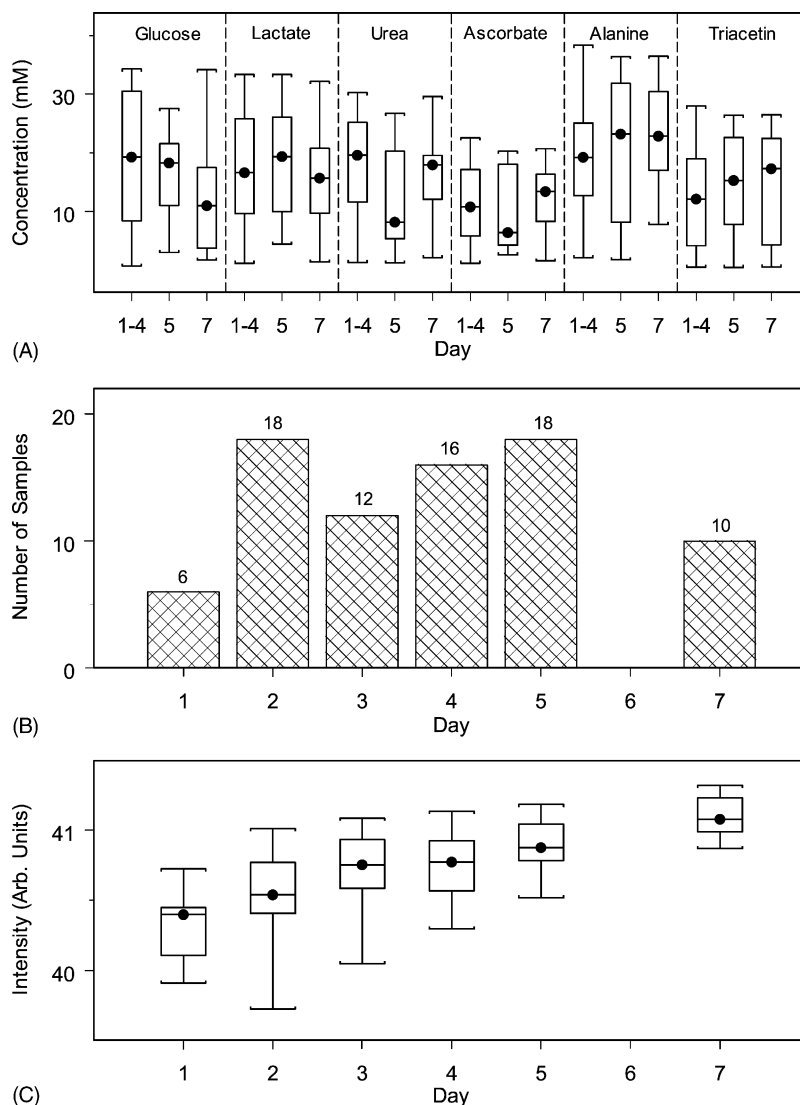


Fig. 1. (A) Box plots displaying concentration distributions for each matrix constituent. Separate distributions are plotted for data collection days 1–4, 5, and 7. Within each box plot, the median concentration is indicated by the solid circle, the box limits are drawn to specify the limits of the upper and lower quartiles of the distribution, and the whiskers indicate the maximum and minimum concentrations. (B) Bar chart indicating the number of samples collected on each day. (C) Box plots displaying the distributions of the maximum intensities in the single-beam spectra of the mixture samples collected each day. The boxes are drawn with the same specifications used in plot A. Clear evidence of spectrometer drift is noted across the 7 days of the data collection.

tion in time between the calibration and prediction data.

For the initial work, further division of the 64 sample calibration set was randomly made into three calibration and three monitoring subsets. The calibration subsets contained 38 samples (114 interferograms)

while the monitoring subsets contained 26 samples (78 interferograms). The replicate interferograms corresponding to a given sample were carried together into the same subset. The calibration subsets were used to build initial PLS regression models while the monitoring subsets were used to test the performance of these

models. This procedure was used to optimize model sizes, digital filtering parameters, and interferogram segment locations. The subsets were recombined and used to build the final PLS regression model with the previously optimized parameters. These final models were applied to the prediction set that was not used anywhere during the training and optimization stages.

3. Results and discussion

3.1. Investigation of spectral information

Fig. 2 is a plot of absorbance as a function of wavenumber for each matrix component at concentrations in the range of 80–100 mM. The glucose spectrum in Fig. 2C reveals three identifiable features corresponding to C–H combination bands near 4400 and 4300 cm^{-1} and an O–H combination band near

4750 cm^{-1} . Previous work has identified the band at 4400 cm^{-1} as the most useful of the three bands for implementing a quantitative analysis for glucose [5,6,8]. Comparison of the spectra in Fig. 2 reveals that the glucose bands are severely overlapped with the bands of the other matrix constituents.

Fig. 3 is a plot of the absorbance spectrum of glucose (solid line). The other plots in this figure show the degree of overlap of each component in the matrix with the spectrum of glucose at the target C–H combination band at 4400 cm^{-1} . It is clear that there is very little selectivity for glucose in this sample matrix.

3.2. Interferogram preprocessing

To facilitate the construction of bandpass filters for use in isolating frequency bands within the interferogram data, it was necessary to reduce the bandwidth of the data from the sampled range of 0–7897 cm^{-1}

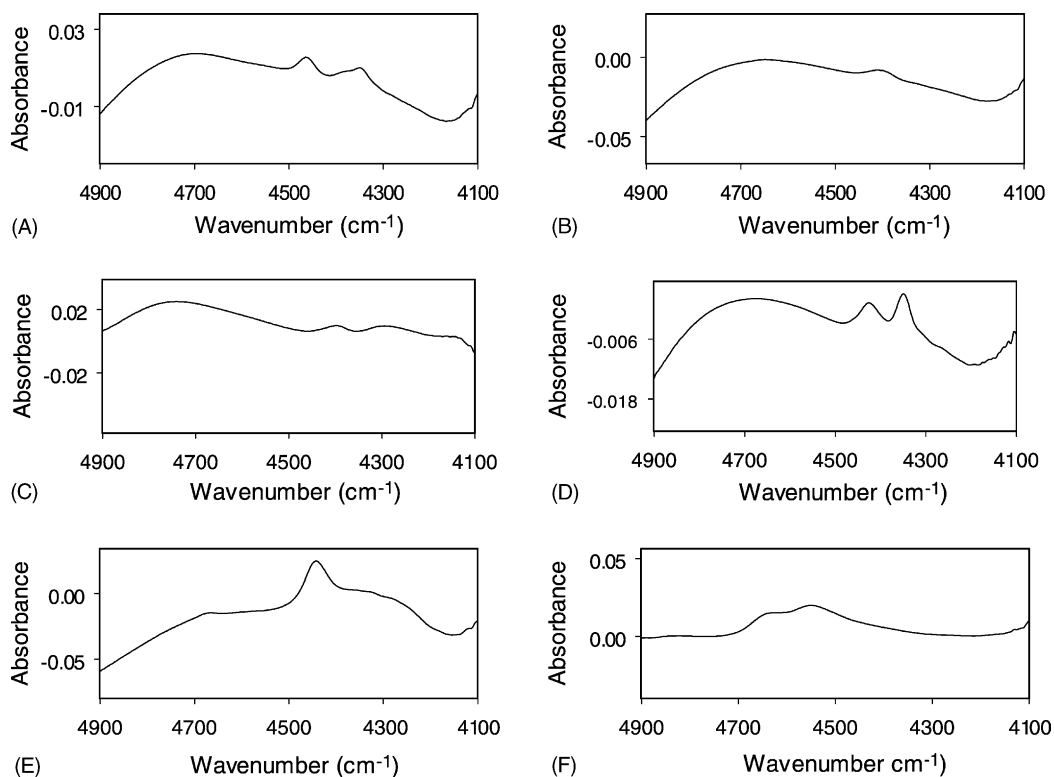


Fig. 2. Absorbance spectra for alanine (A), sodium ascorbate (B), glucose (C), sodium lactate (D), triacetin (E), and urea (F). The concentrations were 100 mM for each species except triacetin, whose concentration was 80 mM. A background single-beam spectrum of phosphate buffer was used in the absorbance calculation.

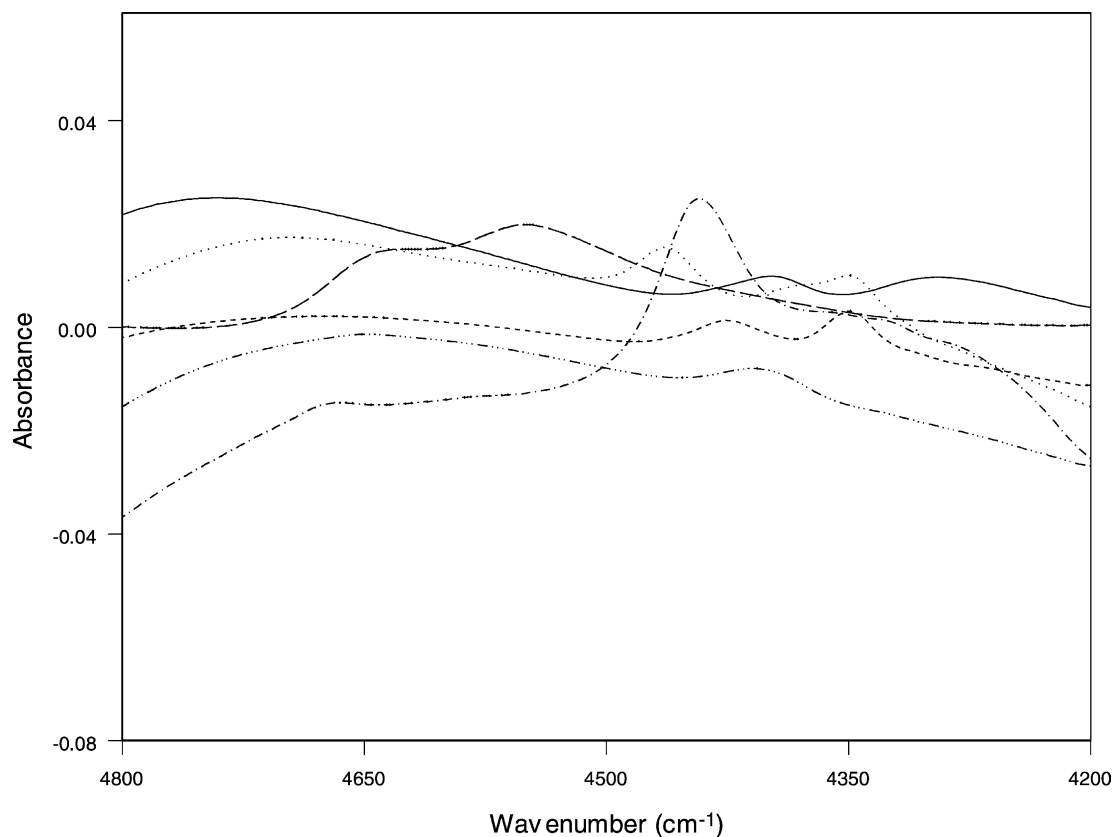


Fig. 3. Absorbance spectra of glucose (solid line) with overlapping spectra of the other components in the matrix. The other plots represent triacetin (— · — · —), ascorbate (·····), lactate (---), urea (— — —), and alanine (···), respectively. There is severe overlap at the analytically relevant C–H combination band of glucose at 4400 cm^{-1} .

to a maximum frequency of 1974 cm^{-1} . The strategy used was to allow the near-IR combination region of $4000\text{--}5000\text{ cm}^{-1}$ to alias onto the $0\text{--}1974\text{ cm}^{-1}$ bandwidth by taking every fourth interferogram point and discarding the rest. The concern in this decimation operation is that the desired $4000\text{--}5000\text{ cm}^{-1}$ data will fold onto noise present at the lower frequencies. Even though an optical K-band interference filter was used to isolate the $4000\text{--}5000\text{ cm}^{-1}$ region during the data collection, previous results have shown that electronic noise exists outside of this region that must be removed before allowing the aliasing to occur [9].

To circumvent this problem, a finite impulse response (FIR) bandpass filter was first applied to the interferogram to isolate the $4000\text{--}5000\text{ cm}^{-1}$ region. Then, the decimation step was performed. The aliasing that results from the decimation procedure can be

expressed as

$$\bar{\nu}_{\text{apparent}} = (2 \times 1974) - (2 \times 3948 - \bar{\nu}_{\text{actual}}) \quad (2)$$

where $\bar{\nu}_{\text{apparent}}$ is the wavenumber after aliasing and $\bar{\nu}_{\text{actual}}$ is the actual wavenumber of the frequency of interest in the unaliased spectrum. For example, a spectral band located at 4500 cm^{-1} will appear at 552 cm^{-1} in the spectrum computed from the decimated interferogram.

Fig. 4A plots an absorbance spectrum obtained from the decimated interferogram corresponding to the first replicate of sample 4. The concentrations were 34.27, 26.58, 10.46, 3.29, 13.85, and 26.31 mM for glucose, lactate, urea, ascorbate, alanine, and triacetin, respectively. The upper X-axis represents the actual frequency while the lower X-axis shows the corresponding decimated frequency values. Comparison

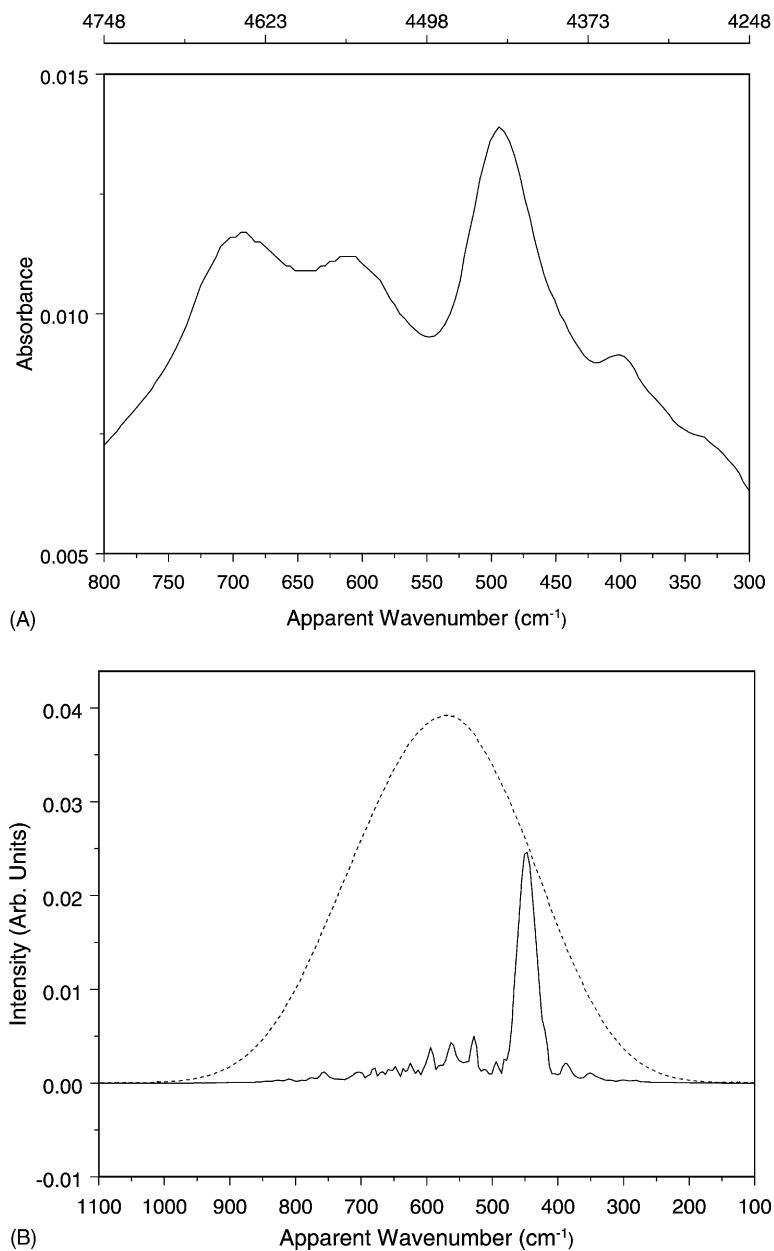


Fig. 4. (A) Mixture absorbance spectrum obtained from the decimated interferogram corresponding to the first replicate of sample 4. A background single-beam spectrum of phosphate buffer was used in the absorbance calculation. The upper X-axis specifies the actual spectral frequencies, while the lower X-axis indicates the corresponding decimated frequencies. (B) Product of the single-beam spectrum of the interferogram used in plot A with the frequency response function of a digital filter positioned at 448 cm^{-1} (solid line). This filter position coincides with the glucose C–H combination band at 4400 cm^{-1} . The unfiltered single-beam spectrum is indicated by the dashed line.

to Fig. 2E reveals that the largest feature in the mixture spectrum is the triacetin band at approximately 4440 cm^{-1} . It is difficult to discern the contribution of glucose to the mixture spectrum. This implies that its signal is obscured by that of triacetin and the other components. The other features in the mixture spectrum represent the additive contributions to the absorbance from the other compounds.

3.3. Overview of data analysis procedures

This research focused on the construction of calibration models for glucose based on the direct use of interferogram data. Fig. 4B plots the product of the single-beam spectrum of the same interferogram used in Fig. 4A with the frequency response function of a digital filter designed to be applied to the interferogram. The single-beam spectrum obtained from the interferogram used in Fig. 4A is represented by the dashed line in Fig. 4B.

The filter used in computing the trace in Fig. 4B was designed by use of a procedure that produces time-dependent FIR filters tailored specifically for application to interferogram data [10,11]. The filter stopband attenuation averaged over $150\text{--}300\text{ cm}^{-1}$ was 21.53 dB, the passband FWHM was 50.14 cm^{-1} , and the average number of coefficients was 105. This filter was centered at 4396 cm^{-1} (448 cm^{-1} decimated frequency), coinciding with the analytically relevant C–H combination band of glucose. The figure shows that the filter attenuates most of the frequency components outside of its passband. In the work described here, filters of this type were used to reduce the frequency content of the interferogram, thereby simplifying the construction of PLS calibration models based on the frequency and intensity data in the interferogram.

As illustrated above, the data analysis procedure begins with filtering raw interferogram data with a digital filter whose frequency response coincides with that of the analyte spectral information. Short segments of the resulting filtered interferograms are then mean centered and used as inputs for building multivariate calibration models based on PLS regression. Variables to be optimized during this procedure include the (1) filter passband position, (2) passband width, (3) length of the interferogram segment filtered, (4) segment starting point relative to the interferogram centerburst, and

(5) number of terms (latent variables or factors) used in the PLS regression model. In addition, the potential benefit of using a concatenated interferogram segment based on the application of two separate filters is evaluated.

3.4. Initial calibration work

Five filters centered on the $448\text{ (}4396\text{) cm}^{-1}$ glucose band and with varying passband FWHM values ($50.14, 69.43, 88.71, 104.14$ and 119.57 cm^{-1}) were generated. An initial study to determine the interaction between the five variables noted above was performed with a factorial design in which each variable was set at two levels. The filter position was fixed at $448\text{ (}4396\text{) cm}^{-1}$. The levels in the design were passband FWHM values of 88.71 and 104.14 cm^{-1} , interferogram segment lengths of 100 and 120 points, segment starting positions of 50 and 75 (ZPD = point 1), and 12 and 14 latent variables. The results of this study were evaluated on the basis of three replicate prediction results of the monitoring sets. The response function used was the standard error of monitoring (SEM). The SEM is calculated by

$$\text{SEM} = \sqrt{\frac{\sum_{i=1}^{n_m} (c_{m,i} - \hat{c}_{m,i})^2}{n_m}} \quad (3)$$

where n_m is the number of interferograms in the monitoring set, $c_{m,i}$ is the actual (prepared) analyte concentration for interferogram i , and $\hat{c}_{m,i}$ is the corresponding analyte concentration predicted by the calibration model. Table 1 displays the results obtained in this study with the variables that were determined to be significant indicated in boldface. This study established two-way interactions between the segment starting position and filter passband width, segment starting position and segment length, and segment starting position and number of latent variables. Among the main effects, the segment starting position and the number of latent variables were found to be significant. No higher order interactions were found to be significant.

Given the presence of multiple interactions among the variables, a joint study of all the parameters was undertaken with the five filters. The segment starting position was varied between points 25 and 175 in steps of 25 points, the segment length was varied from 100

Table 1
Results from factorial design study

Term ^a	Computed effect ^b	P-value ^c
<i>w</i>	0.0131	0.458
<i>s</i>	0.1331	0.000
<i>f</i>	-0.1119	0.000
<i>k</i>	0.0044	0.834
<i>w</i> × <i>s</i>	0.0531	0.006
<i>w</i> × <i>f</i>	0.0206	0.268
<i>w</i> × <i>k</i>	0.0294	0.106
<i>s</i> × <i>f</i>	0.0456	0.015
<i>s</i> × <i>k</i>	-0.0481	0.010
<i>f</i> × <i>k</i>	-0.0181	0.343
<i>w</i> × <i>s</i> × <i>f</i>	0.0056	0.780
<i>w</i> × <i>s</i> × <i>k</i>	0.0294	0.115
<i>w</i> × <i>f</i> × <i>k</i>	0.0169	0.367
<i>s</i> × <i>f</i> × <i>k</i>	0.0094	0.658
<i>w</i> × <i>s</i> × <i>f</i> × <i>k</i>	0.0069	0.727

^a Symbols: *w*—FWHM (cm⁻¹) of target passband; *s*—interferogram segment starting point; *f*—number of PLS factors; *k*—interferogram segment length.

^b The response variable used to compute the effects was the standard error of monitoring (SEM). The computed standard error in the effects was 0.02. Effects judged to be significant on the basis of *P*-values at the 95% confidence level are shown in boldface.

^c *P*-values in boldface are judged to be significant.

to 150 points in steps of 10 points, and the number of latent variables ranged from 10 to 22.

For each combination of filter width, segment length, and segment starting position, the optimal number of latent variables was taken as the minimum number that produced a value of SEM that was not statistically different from the minimum SEM at the 95% confidence level. For this calculation, SEM was pooled over the three monitoring sets.

Using the optimal number of latent variables for each combination of the other variables, the pooled SEM values were sorted and the best model was selected. These optimal settings were then used to build a final model by use of the full calibration set of 64 samples. The resulting model was used to predict the concentration of glucose in the prediction set. This set was not used anywhere during the model optimization steps. The resulting standard error of calibration (SEC) and standard error of prediction (SEP) obtained in this study were 0.534 and 0.529 mM, respectively. The values of SEC and SEP are computed in an analogous manner to SEM, with the SEC value adjusted for the loss of degrees of freedom corresponding to the number of latent variables.

3.5. Extended investigation of filter position

An extended investigation of the effect of the filter position was conducted next. Eighty-nine filters were generated at two levels of passband width to cover the spectral range of 4280–4720 (332–772) cm⁻¹ in steps of 5 cm⁻¹. This spectral range encompasses all three of the glucose absorption bands (4300, 4400 and 4750 cm⁻¹). The passband widths of these filters were 50.14 and 69.43 cm⁻¹. The purpose of this study was to evaluate other candidate spectral regions for determining glucose as well as provide direction in choosing filters to be used in adding a second filter to the analysis.

For each filter, the interferogram segment position, segment length, and number of PLS latent variables were varied over the same ranges as described above. The results were ranked and a cutoff pooled SEM of 0.60 mM was selected. For each combination of filter and interferogram segment variables that met this criterion, the optimal number of latent variables was determined by the *F*-test procedure described previously. The results of this study showed that the spectral region of 4350–4450 cm⁻¹ is required for the analysis of glucose and that 50.14 cm⁻¹ is the better of the two filter widths evaluated.

On the basis of the above study, 51 filters were generated next in the range of 4350–4450 cm⁻¹ with a spacing of 2 cm⁻¹. The filters had a passband width of 50.14 cm⁻¹. The optimization of the interferogram segment and the number of latent variables to use with these filters was performed as described previously. Results were again sorted on the basis of the pooled SEM and the two best performing combinations of the filter and interferogram segment variables were selected. For these cases, final models were computed with the full calibration set and the resulting models were applied to the prediction set. For the cases corresponding to the above two models, Table 2 lists the filter and segment variables, number of latent variables, SEC, and SEP.

3.6. Evaluation of models based on two filters

A study was performed next to evaluate the utility of models constructed by use of two filters. In this approach, each filter is applied to an optimal segment of the raw interferogram and the two resulting filtered

Table 2

Results from models based on one filter

Filter position ^a (cm ⁻¹)	Filter width ^b (cm ⁻¹)	Segment location ^c	Segment length	No. PLS factors	SEC ^d (mM)	SEP ^d (mM)	SEC ^e (mM)	SEP day 5 (mM)	SEP day 7 (mM)
4396 (448)	50.14	75/204	130	13	0.53	0.53	0.54	0.47	0.54
4422 (474)	50.14	75/194	120	13	0.44	0.47	0.44	0.57	0.33

^a The number in parentheses indicates the decimated frequency.^b Filter width specified as the FWHM of the passband.^c Point 1 specifies the location of the interferogram centerburst.^d Result based on randomly selected calibration/prediction sets.^e Result based on calibration data from days 1 to 4.

segments are concatenated and submitted to the PLS calculation. To optimize the two-filter models, the two best performing filter/segment combinations found in the initial study and described in Table 2 were selected. In turn, each of these filters was designated as the first filter of the set of two, and the remaining filters in the group of 51 were then evaluated for use in combination with the first filter. The interferogram segment variables optimized previously for the first filter were retained, and a grid search optimization procedure was applied to find the best settings for use with the second filter. The segment starting position, the segment length, and the number of latent variables were varied between points 25 and 100 in steps of 25, 100–150 points in steps of 10, and 10–20 latent variables, respectively.

The pooled SEM was calculated for each combination, and the top 10 performing models were selected. The number of latent variables was optimized for these models by use of the *F*-test described previously, and the three best performing two-filter models were selected. Final models were then computed by

use of the full calibration set, and the resulting models were applied to the prediction set. Table 3 summarizes the calibration and prediction results for the two-filter models.

Comparing the results in Tables 2 and 3, it is observed that the use of two filters improves the SEP by 19% when the second filter is used in conjunction with the first filter centered at 4396 cm⁻¹. Adding a second filter to the first filter at 4422 cm⁻¹ provides no benefit, however.

3.7. Evaluation of model robustness to instrumental drift

The next approach was to build a model based on the data collected on days 1–4, followed by prediction of the data from days 5 and 7. In this case, the training set contained 52 samples (156 interferograms). The prediction sets contained 18 samples (54 interferograms) and 10 samples (30 interferograms) for the data collected on days 5 and 7, respectively. By use of this procedure, it is possible to evaluate whether the

Table 3

Results from models based on two filters

First filter position ^{a,b} (cm ⁻¹)	Second filter position ^b (cm ⁻¹)	Second segment location ^c	Second segment length	No. PLS factors	SEC ^d (mM)	SEP ^d (mM)	SEC ^e (mM)	SEP day 5 (mM)	SEP day 7 (mM)
4396 (448)	4432 (484)	50/149	150	15	0.36	0.43	0.36	0.42	0.48
4396 (448)	4446 (500)	50/149	150	15	0.40	0.43	0.40	0.39	0.50
4422 (474)	4450 (502)	75/194	120	15	0.48	0.47	0.44	0.56	0.56

^a The segment parameters associated with the first filter are listed in Table 2.^b The number in parentheses indicates the decimated frequency.^c Point 1 specifies the location of the interferogram centerburst.^d Result based on randomly selected calibration/prediction sets.^e Result based on calibration data from days 1 to 4.

interferogram-based models are susceptible to the effects of instrumental drift such as that suggested by Fig. 1C.

The previously optimized filter and segment variables were used with the calibration data from days 1 to 4 to build models based on one and two filters. The results are presented in the last three columns of Tables 2 and 3 for the models based on one and two filters, respectively.

Fig. 5A and B are correlation plots of the predicted versus the prepared concentrations for the calibration and prediction sets, respectively, that were obtained with the filter positioned at 4396 cm^{-1} . Open circles and triangles are used in Fig. 5B to differentiate the prediction samples from days 5 and 7, respectively. Fig. 6A and B are similar plots obtained with the two-filter model based on filters positioned at 4396 and 4432 cm^{-1} . For the prediction data and the same

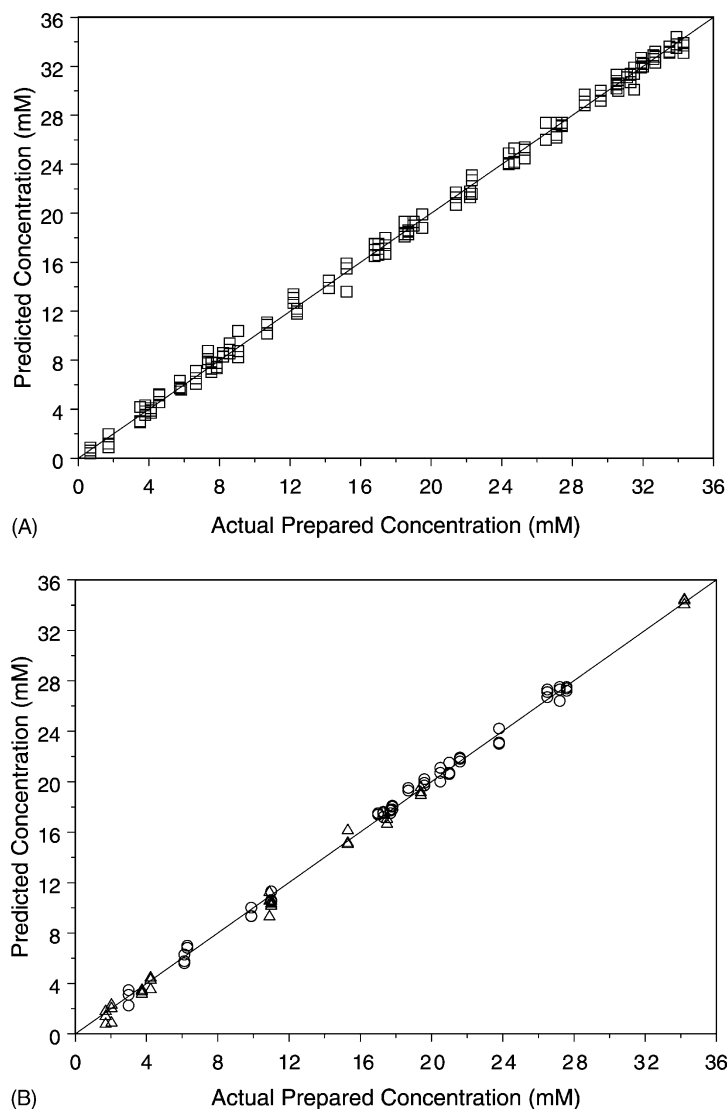


Fig. 5. Correlation plots of predicted versus prepared glucose concentration for (A) the calibration data from days 1 to 4 and (B) the prediction data from day 5 (○) and day 7 (△). The calibration model based on a single filter positioned at 4396 cm^{-1} was used. Calibration and prediction statistics for this model are listed in Table 2.

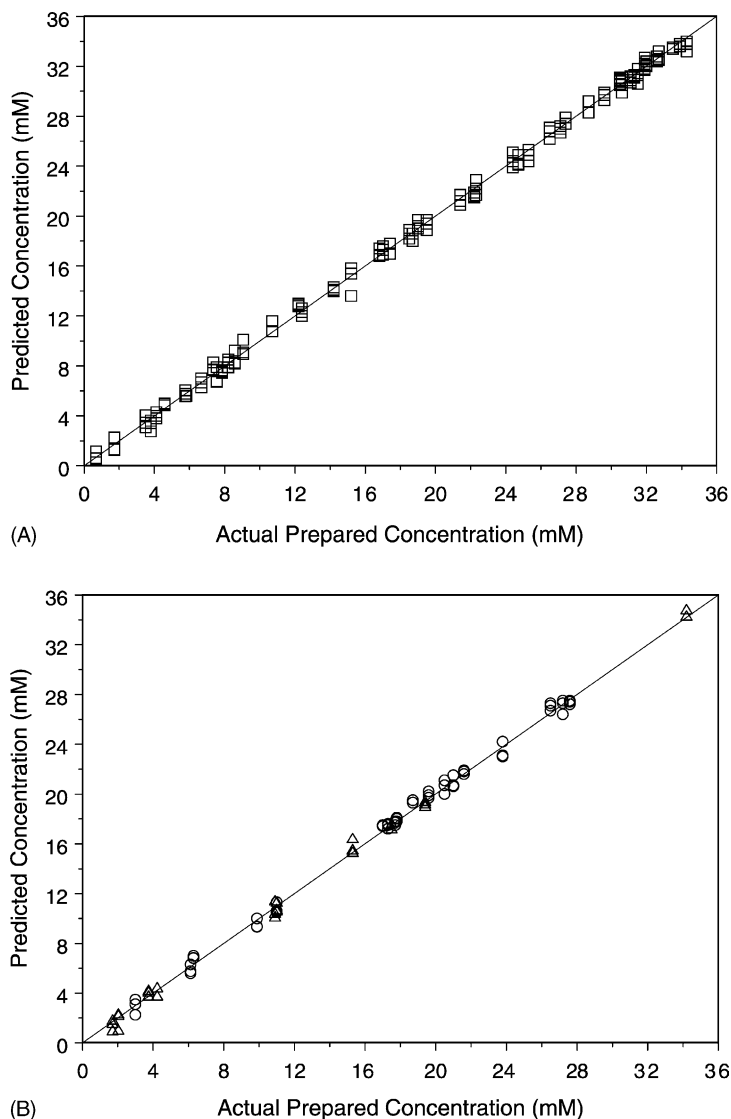


Fig. 6. Correlation plots of predicted versus prepared glucose concentration for (A) the calibration data from days 1 to 4 and (B) the prediction data from day 5 (○) and day 7 (△). The calibration model based on two filters positioned at 4396 and 4432 cm^{-1} was used. Calibration and prediction statistics for this model are listed in Table 3.

one- and two-filter models, respectively, Fig. 7A and B plots the residuals versus the predicted concentrations. Fig. 8A and B are corresponding plots of residuals versus the time sequence of the data collection. In Figs. 7 and 8, separate symbols are again used to differentiate data from days 5 and 7.

Inspection of Tables 2–3 and Figs. 5–8 reveals that the models perform well in predictions outside of the

time span of the calibration data. Prediction performance is essentially the same as in the case where the calibration data spans the prediction data in time. Both sets of residual plots are random in character and show no obvious trending. As observed in the initial study, the models based on two filters slightly outperform the one-filter models. These results confirm that the interferogram-based calibration models

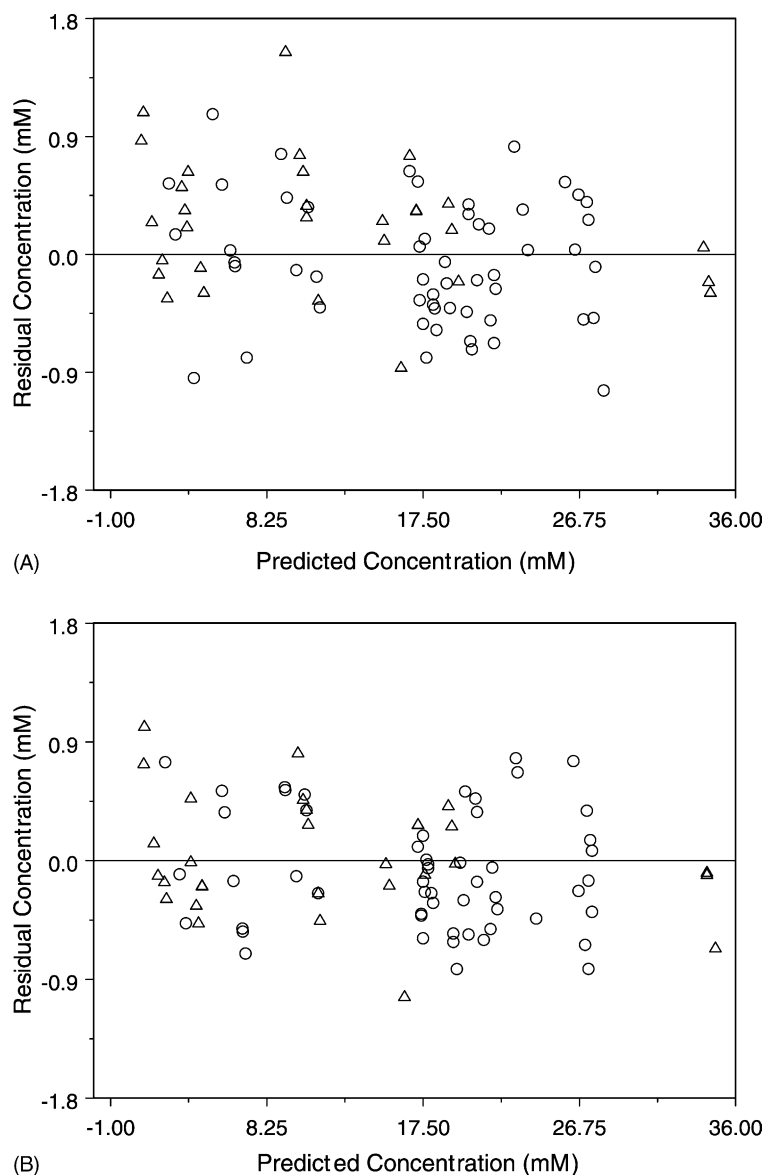


Fig. 7. Plot of residuals with respect to predicted glucose concentrations for the prediction data from day 5 (○) and day 7 (△). Plots A and B correspond to the one- and two-filter interferogram-based models depicted in Figs. 5 and 6, respectively.

are sufficiently robust to instrumental variation to be used in an external prediction.

3.8. Single-beam and absorbance spectral analysis

To place the results presented previously in context, a parallel study was performed to build calibration

models with both single-beam and absorbance spectral data. For this study, the same randomly selected calibration, monitoring, and prediction sets used in the initial work with the interferogram data were employed.

For the single-beam spectral analysis, the intensity variation caused by uncontrollable instrumental changes was removed through spectral normalization.

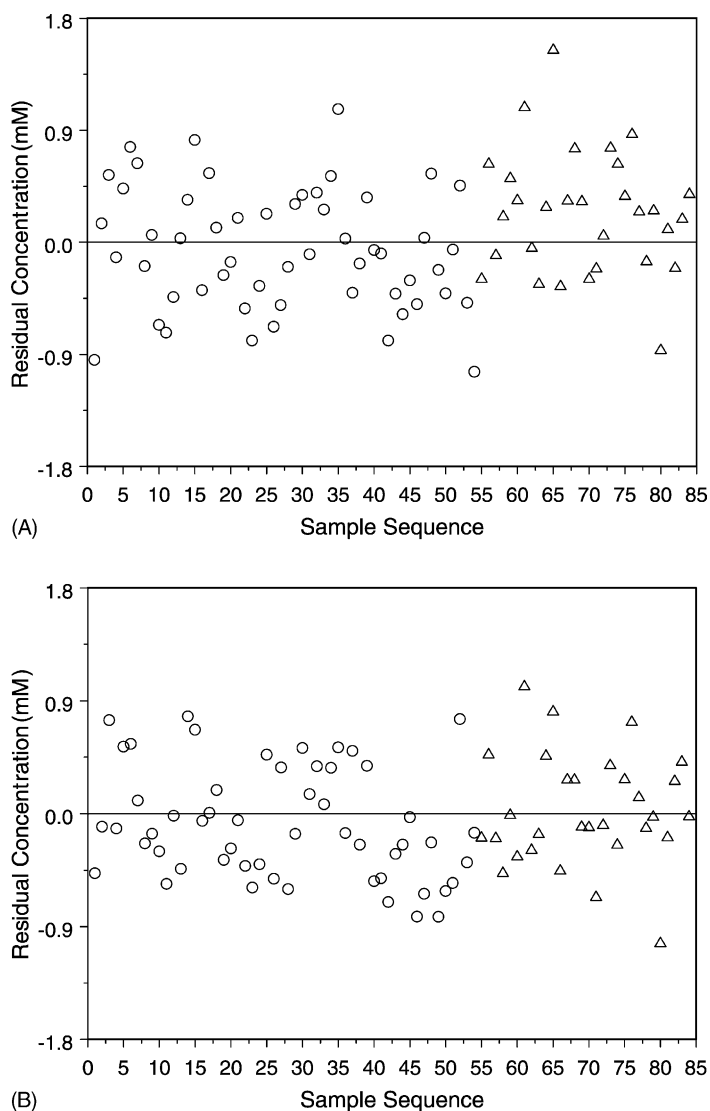


Fig. 8. Plot of residuals with respect to the time sequence of the data collection for the prediction data from day 5 (○) and day 7 (Δ). Plots A and B correspond to the one- and two-filter interferogram-based models depicted in Figs. 5 and 6, respectively.

The single-beam spectra were normalized by dividing the values of individual spectral points by the root sum of squares of the intensity values in the corresponding spectrum.

For the spectral-based analysis, the variables requiring optimization are the number of latent variables and the spectral region submitted to the PLS algorithm. A grid search procedure was adopted to study the spectral region of $4850\text{--}4100\text{ cm}^{-1}$ by varying the size and

location of the spectral range systematically. The size of the spectral range was varied from $100\text{ to }700\text{ cm}^{-1}$ in steps of 50 cm^{-1} . For a given range size, the spectral range was shifted across $4850\text{--}4100\text{ cm}^{-1}$ in steps of 10 cm^{-1} . Optimization was conducted by varying the number of latent variables from 6 to 15. As before, the value of SEM pooled across the three monitoring sets was used to sort the results and identify the best model. The optimal number of latent variables was

Table 4
Comparison of spectral and interferogram processing

Method	Spectral range/filter position (cm ⁻¹)	Number of PLS factors	SEC ^a (mM)	SEP ^a (mM)	SEC ^b (mM)	SEP day 5 (mM)	SEP day 7 (mM)
Absorbance spectra	4440–4240	10	0.42	0.44	0.42	0.44	0.46
Single-beam spectra	4450–4200	9	0.45	0.55	0.46	0.50	0.51
Interferogram (one filter)	4396	13	0.53	0.53	0.54	0.47	0.54
Interferogram (two filters)	4396, 4432	15	0.36	0.43	0.36	0.42	0.48

^a Result based on randomly selected calibration/prediction sets.

^b Result based on calibration data from days 1 to 4.

determined by use of the *F*-test procedure described previously. The final calibration model was then computed with the full 64 sample calibration set. This model was used to predict the concentration of glucose in the prediction set. Table 4 lists the spectral range, number of latent variables, and the values of SEC and SEP for the optimal model. The best results from the one- and two-filter interferogram-based analyses are also included in Table 4 to facilitate comparisons.

Subsequently, the same spectral range and number of latent variables was used with the calibration set based on days 1–4 and the prediction sets from days 5 and 7. The values of SEC and SEP for these data sets are also included in Table 4.

A similar procedure was used in an analysis of absorbance spectra. For each sample, the most recently collected background spectrum of phosphate buffer was used in computing the absorbance values. The same grid search optimization procedure described above was employed with the absorbance data. As before, the spectral range and number of latent variables were optimized with the randomly selected calibration/monitoring sets. Final models were computed with the full 64 sample calibration set and applied to the corresponding prediction set. Models were also computed with the calibration set based on data from days 1 and 4 and applied to the prediction data from days 5 and 7. Both sets of calibration and prediction results are reported in Table 4.

Inspection of Table 4 reveals that the absorbance spectral processing shows slightly improved prediction results over the analysis based on single-beam spectra. Overall, prediction results are similar for the interferogram- and spectral-based calibration models. This study demonstrates that the interferogram processing approach for the determination of glucose is

competitive with the conventional absorbance spectral analysis.

4. Conclusions

The similarity in the results of the spectral- and interferogram-based analyses provides validation to the concept of a dedicated glucose analyzer based on a short-scan interferometer design. Even with the use of two filters applied to separate interferogram segments, a contiguous segment of only 155 interferogram points was required for the analysis. Such an approach may help to overcome current impediments to the development of a rugged and low-cost instrument design for use in a noninvasive glucose measurement. The use of direct interferogram processing also does not require a separate background or reference measurement. This is important, especially from the standpoint of the ultimate goal of a noninvasive glucose determination where it is not feasible to measure glucose-free background spectra.

The use of two filters in the interferogram-based analysis was found to provide a small but consistent improvement in the results for the determination of glucose in the presence of interfering species. This suggests that additional information pertaining to the sample matrix in the concatenated interferogram segment allows the PLS algorithm to better decompose the overlapping contributions of the matrix constituents.

One limitation encountered in this research was the width of the filters that could be successfully generated. Filters with passband FWHM values less than 50 cm⁻¹ were difficult to construct that also possessed good attenuation in the stopbands. Further work with

an alternate filter design method is suggested to evaluate the potential benefit of narrower filters.

Finally, the optimization procedures used in this work were limited in that a stepwise strategy was employed in which the first filter was optimized, followed by the investigation of the second filter. A better approach would be to employ a global optimization of several filters at once. Such a strategy would also have fewer restrictions on the number of levels of passband position and width than were employed in this work.

Acknowledgements

Lin Zhang and Jun Chen are acknowledged for collecting the interferogram data used in this research. Funding for this work was provided by the National Institutes of Health under grant DK60657. Portions of this research were presented at the 8th International Conference on Chemometrics in Analytical Chemistry, Seattle, WA, September, 2002.

References

- [1] H.M. Heise, in: D.M. Fraser (Ed.), *Biosensors in the Body: Continuous In Vivo Monitoring*, Wiley, Chichester, UK, 1997, pp. 79–116.
- [2] C. Fischbacher, K.-U. Jagemann, K. Danzer, U.A. Muller, L. Papenkordt, J. Schuler, *Fresenius J. Anal. Chem.* 359 (1997) 78.
- [3] J.J. Burmeister, M.A. Arnold, G.W. Small, *Diabetes Technol. Ther.* 2 (2000) 5.
- [4] P.R. Griffiths, J.A. de Haseth, *Fourier Transform Infrared Spectrometry*, Wiley, New York, 1986.
- [5] M.J. Mattu, G.W. Small, M.A. Arnold, *Appl. Spectrosc.* 51 (1997) 1369.
- [6] M.J. Mattu, G.W. Small, M.A. Arnold, *Anal. Chem.* 69 (1997) 4695.
- [7] D.M. Haaland, E.V. Thomas, *Anal. Chem.* 60 (1988) 1193.
- [8] M.A. Arnold, G.W. Small, *Anal. Chem.* 62 (1990) 1457.
- [9] N.A. Cingo, G.W. Small, M.A. Arnold, *Vib. Spectrosc.* 23 (2000) 103.
- [10] G.W. Small, A.C. Harms, R.T. Kroutil, J.T. Ditillo, W.R. Loerop, *Anal. Chem.* 62 (1990) 1768.
- [11] M.J. Wabomba, G.W. Small, *Chemom. Intell. Lab. Syst.*, submitted for publication.